Chapter 3
Computer-Aided Analysis of Acoustic Propagation

3.1 INTRODUCTION

For the symmetry classes considered in Chapter 2, it was easy to solve the phase velocities (the eigenvalues of the Christoffel equation) only for the simplest, usually principal, axis directions. For most of these cases, it is possible to determine the eigenvalues by inspection of the stiffness matrix. For an arbitrary propagation direction, which requires solving the characteristic equation to find the phase velocities, the computation becomes complex and cumbersome. An important exception occurs when the propagation is in a principal plane that contains a pure shear mode. In this chapter, we develop computer-aided computational techniques that significantly ease the burden of finding the eigenvalues and that provide insight into the acoustic properties of symmetry classes. Velocity curves are drawn for several important crystals.

As a consequence of anisotropy, the energy does not propagate in a direction parallel to the wave propagation. This phenomena, though present in optically anisotropic as well as acoustically anisotropic media, is much more pronounced in the acoustic case because of the large anisotropies that are common in acoustic modes. The angle between the energy velocity (which is identical to the group velocity) and the propagation direction $\hat{\mathbf{l}}$ is called the *power flow angle*. This angle depends on the *shape* of the inverse velocity (slowness) curve. We use computer-aided techniques to determine the power flow angle, and we examine some important crystals.

3.2 COMPUTER SOLUTION OF THE CHRISTOFFEL EQUATION

The structure of the acoustic equations admits three possible solutions (two in the case of a shear degeneracy). Each mode has associated with it a particular stiffness constant. For simple directions (e.g., the major axes), the required stiffness component can sometimes be found from inspection of the stiffness matrix; for off-axis directions, however, the solutions are combinations of c values, and their determination is usually quite cumbersome.

Figure 3.1 shows a computer program, called *Christoffel*, that computes three stiffness constants. The program is written in the True BASIC language for the IBM PC. We chose this language because it allows easy manipulation of matrices and closely emulates HP BASIC. The program solves the Christoffel equation for a given propagation direction and material stiffness matrix. Three-dimensional space is cut into user-defined planes with predefined abscissa and ordinate, which are required to be orthogonal. The input data consist of the 6×6 stiffness matrix, the density of the material, and these reference axes. The program plots the acoustic phase velocity (the eigenvalues of the Christoffel matrix) as a function of the angle referred to the reference axes.

We calculate the Christoffel matrix, which contains all the required information, not by rotating $\mathbf{c}$ but by performing the rules outlined in (2.48) to (2.51).

The program is divided into five blocks:

1. *Input of the stiffness matrix and the density*. The form of the stiffness matrix determines the symmetry properties of the propagation, and thus there is no need to specify the symmetry class.

2. *Definition of the propagation direction*. We form two perpendicular axes that can be positioned arbitrarily in three space. The propagation direction $\hat{\mathbf{l}}$ varies from one axis to the other as the angle θ varies from 0 to 90°.

3. *Formation of the Christoffel matrix*. We form the product:

$$\Gamma = \tilde{\mathbf{l}}:\mathbf{c}:\mathbf{l} \tag{3.1}$$

where $\mathbf{l}$ is the 6×3 gradient matrix operator, and its transpose $\tilde{\mathbf{l}}$ is the 3×6 divergence matrix operator.

4. *Solution of the characteristic equation*.

$$|\Gamma - \lambda| = 0 \tag{3.2}$$

5. Because Γ is a 3×3 matrix, solving (3.2) reduces to *solving a cubic equation*.

```
1000  !THIS PROGRAM PLOTS THE THREE ACOUSTIC VELOCITIES
1030  OPTION BASE 1
1060  LIBRARY "GRAPHLIB" !INTERNAL GRAPHICS LIBRARY
1090  DIM T33(3,3) !CHRISTOFFEL MATRIX
1120  DIM L13(1,3) !DIRECTION OF PROPAGATION
1150  DIM CL63(6,3)!INTERMEDIATE PRODUCT
1180  DIM ROOT(3)!ROOTS OF THE CHRISTOFFEL MATRIX
1210  DIM L36(3,6),L63(6,3)!DIVERGENCE AND GRADIENT MATRIX OPERATORS
1240  DIM C66(6,6) !STIFFNESS MATRIX
1270  DIM R1(3,3) !ROTATION MATRIX
1300  DIM AA(3),BB(3) !ABSCISSA AND ORDINATE OF GRAPH
1330  DIM SS(1,3) !ROTATES THE PROPAGATION VECTOR FROM ABSCISSA TO ORDINATE
1360  DIM VEL(3) ! THE PHASE VELOCITIES OF THE THREE MODES
1390  MAT READ C66 !DATA FOR GALLIUM PHOSPHIDE
1420   DATA 140,62,62,0,0,0
1450   DATA 62,140,62,0,0,0
1480   DATA 62,62,140,0,0,0
1510   DATA 0,0,0,70,0,0
1540   DATA 0,0,0,0,70,0
1570   DATA 0,0,0,0,0,70
1600  !STIFFNESS TENSOR
1630  LET DENS=4.13  !DENSITY OF THE CRYSTAL IN GM/CC
1660  !THIS ROUTINE SETS THE AXES
1690  INPUT PROMPT "X AXIS IS:": AA(1),AA(2),AA(3)
1720  INPUT PROMPT "Y AXIS IS:":  BB(1),BB(2),BB(3)
1750  LET  AN=(AA(1)^2+AA(2)^2+AA(3)^2)^.5
1780  LET  BN=(BB(1)^2+BB(2)^2+BB(3)^2)^.5
1810  LET DOT=AA(1)*BB(1)+AA(2)*BB(2)+AA(3)*BB(3)
1840  IF ABS(DOT)>1E-3 THEN GOTO 1900
1870  GOTO 1960 !AXES MUST BE ORTHOGONAL
1900  PRINT "AXES ARE NOT ORTHOGONAL"
1930  GOTO 4330
1960  LET  R1(1,1)=AA(1)/AN
1990  LET  R1(1,2)=AA(2)/AN
2020  LET  R1(1,3)=AA(3)/AN
2050  LET  R1(2,1)=BB(1)/BN
2080  LET  R1(2,2)=BB(2)/BN
2110  LET  R1(2,3)=BB(3)/BN
2140  LET  R1(3,1)=R1(1,2)*R1(2,3)-R1(2,2)*R1(1,3)
2170  LET  R1(3,2)=R1(2,1)*R1(1,3)-R1(2,3)*R1(1,1)
2200  LET  R1(3,3)=R1(1,1)*R1(2,2)-R1(2,1)*R1(1,2)
2230  SET MODE "HIRES" !GRAPHICS RESOLUTION
2260  !THIS IS THE MAIN LOOP
2290  LET  XX=8
2320  OPEN #1: SCREEN .1,.9,0,1
2350  SET WINDOW -1.0*XX,1.0*XX,-XX,XX
2380  CALL FRAME
2410  CALL AXES
2440  CALL TICKS(.5,.5)
2470  FOR N=1 TO 3 !THERE ARE THREE MODES
2500  FOR THETA=0 TO 2*PI STEP PI/180
2530  LET  SS(1,1)=COS(THETA)
2560  LET  SS(1,2)=SIN(THETA)
2590  LET  SS(1,3)=0
2620  MAT L13=SS*R1  ! DIRECTION OF PROPAGATION
2650  !L36(3,6) IS THE DIVERGENCE MATRIX OPERATOR
2680  LET L36(1,1)=L13(1,1)
2710  LET L36(2,2)=L13(1,2)
2740  LET L36(3,3)=L13(1,3)
2770  LET L36(1,5)=L13(1,3)
```

Figure 3.1 Program listing for calculation of eigenvalues for arbitrary crystal symmetry.

```
2800  LET L36(1,6)=L13(1,2)
2830  LET L36(2,4)=L13(1,3)
2860  LET L36(2,6)=L13(1,1)
2890  LET L36(3,4)=L13(1,2)
2920  LET L36(3,5)=L13(1,1)
2950  !THE TRANSPOSE OF L36, L63(6,3), IS THE GRADIENT MATRIX OPERATOR
2980  MAT L63 = TRN(L36)
3010  MAT CL63 = C66*L63
3040  MAT T33 = L36*CL63  !THIS IS THE CHRISTOFFEL MATRIX!!!
3070  !THIS ROUTINE SOLVES THE CHARACTERISTIC EQUATION
3100  LET P=-(T33(1,1)+T33(2,2)+T33(3,3))
3130  LET Q=T33(1,1)*T33(3,3)+T33(1,1)*T33(2,2)+T33(2,2)*T33(3,3)
3160  LET Q=Q-(T33(2,1)^2+T33(2,3)^2+T33(3,1)^2)
3190  LET R=T33(1,1)*T33(3,2)^2+T33(3,3)*T33(1,2)^2+T33(2,2)*T33(1,3)^2
3220  LET R=R-T33(1,1)*T33(2,2)*T33(3,3)-2*T33(1,2)*T33(1,3)*T33(2,3)
3250  !THIS ROUTINE SOLVES FOR THE ROOTS OF A CUBIC EQUATION
3280  LET A=(3*Q-P*P)/3
3310  LET B=(2*P*P*P-9*P*Q+27*R)/27
3340  LET X=0
3370  IF B=0 THEN GOTO 3820
3400  LET A2=B*B/4+A*A*A/27
3430  IF A2>0 THEN LET A2=0
3460  LET A2=-A2
3490  LET D=SQR(A2)
3520  LET A3=-B/2
3550  LET R2=SQR(A3*A3+D*D)
3580  IF A3<0 THEN GOTO 3670
3610  LET P1=ATN(D/A3)
3640  GOTO 3700
3670  LET P1=(PI)-ATN(D/A3)
3700  LET R2=EXP(LOG(R2)/3)
3730  LET P1=P1/3
3760  LET X=R2*COS(P1)
3790  LET X=X*2
3820  LET ROOT(1)=X-P/3
3850  LET Z=(P+ROOT(1))/2
3880  LET SP=Z*Z+R/ROOT(1)
3910  LET SP=ABS(SP)
3940  LET  ROOT(2)=-Z+SQR(SP)
3970  LET  ROOT(3)=-Z-SQR(SP)
4000  !THE THREE ROOTS ARE THE REQUIRED STIFFNESS CONSTANTS OF THE MODES
4030  !PRINT ROOT(1), ROOT(2), ROOT(3) , THETA*180/PI
4060  LET VEL(1)=(ROOT(1)/DENS)^.5
4090  LET VEL(2)=(ROOT(2)/DENS)^.5
4120  LET VEL(3)=(ROOT(3)/DENS)^.5
4150  LET X=(VEL(N)*COS(THETA))
4180  LET Y=(VEL(N)*SIN(THETA))
4210  PLOT  X, Y;
4240  NEXT THETA
4270  NEXT N
4300  CLOSE #1
4330  END
```

We obtain the phase velocities by simply dividing each number by the density and taking the square root.

Lines 1420 to 1630 input data consisting of the **c** matrix and the density of the material. All required information concerning the symmetry class is contained in **c**.

Lines 1690 to 2200 set the axes: We define a rotation matrix, $\mathbf{R}_1$:

$$\mathbf{R}_1 = \begin{bmatrix} x_1 & x_2 & x_3 \\ y_1 & y_2 & y_3 \\ z_1 & z_2 & z_3 \end{bmatrix} \begin{matrix} \leftarrow \text{abscissa} \\ \leftarrow \text{ordinate} \\ \leftarrow \hat{\mathbf{z}} = \hat{\mathbf{x}} \times \hat{\mathbf{y}} \end{matrix} \tag{3.3}$$

where $\hat{\mathbf{x}} = (x_1, x_2, x_3)$, $\hat{\mathbf{y}} = (y_1, y_2, y_3)$, and $\hat{\mathbf{z}} = \hat{\mathbf{x}} \times \hat{\mathbf{y}}$ is the cross product of unit vectors $\hat{\mathbf{x}}$ and $\hat{\mathbf{y}}$.

It is the user's responsibility to ensure that $\hat{\mathbf{x}}$ and $\hat{\mathbf{y}}$ are perpendicular, but $\mathbf{x}$ and $\mathbf{y}$ need not be normalized.

We next define a vector $\mathbf{S}$:

$$\mathbf{S} = (\cos\theta, \sin\theta, 0) \tag{3.4}$$

As θ ranges from 0 to 90°, the propagation vector $\hat{\mathbf{l}}$ rotates from the abscissa to the ordinate:

$$\hat{\mathbf{l}} = \mathbf{S} \cdot \mathbf{R}_1 \tag{3.5}$$

Similarly, if $\mathbf{S}$ is defined as

$$\mathbf{S} = (0, \cos\theta, \sin\theta) \tag{3.6}$$

then, as θ ranges from 0 to 90°, $\hat{\mathbf{l}}$ rotates from the y- to the z-axis. This may be useful if we need to view orthogonal planes without redefining the axes.

As an example, consider the plane defined by the axes: Let $\hat{\mathbf{x}}_1 = (1, 1, 1)$ and $\hat{\mathbf{y}} = (-2, 1, 1)$; then $\hat{\mathbf{z}} = (0, -1, 1)$. If θ is defined as in (3.5), then

$$\hat{\mathbf{l}} = \mathbf{S} \cdot \mathbf{R}_1 = (\cos\theta - 2\sin\theta, \cos\theta + \sin\theta, \cos\theta + \sin\theta)$$

At $\theta = 0$, we find immediately that $\hat{\mathbf{l}} = (1, 1, 1)$, and at $\theta = 90°$, $\hat{\mathbf{l}} = (-2, 1, 1)$ as expected. Alternatively, if $\theta = 0$ is defined as the y-axis, we would have

$$\hat{\mathbf{l}} = \mathbf{S} \cdot \mathbf{R}_1 = (-2\cos\theta, \cos\theta - \sin\theta, \cos\theta + \sin\theta)$$

At $\theta = 0$, $\hat{\mathbf{l}} = (-2, 1, 1)$, and at $\theta = 90°$, $\hat{\mathbf{l}} = (0, -1, 1)$ (the z-axis).

Line 2500 begins the main calculation loop. The Christoffel matrix is formed in lines 2680 to 3040 by following (2.48) and (2.49). For an

arbitrary propagation direction, the Christoffel matrix will contain nine nonzero components (six of which are independent, because the matrix is always symmetric). Thus, the solution to the characteristic equation involves finding the roots of the third-order polynomial. This operation is performed in lines 3280 to 3970 by a standard algorithm that computes the roots in closed form. The result is the three stiffness components corresponding to the three acoustic modes. The velocities are found by dividing each c component by the density and then taking the square root.

In this relatively simple formulation, no attempt has been made to label a root as a particular mode. However, because root(1) is usually the largest root, it corresponds to the logitudinal mode, and root(2) and root(3) correspond to the fast and slow shear modes, respectively. As the angle sweeps through a direction of shear degeneracy, these values flip, creating the appearance of a discontinuity in the individual curves. A more rigorous approach would determine the polarization of a particular mode and require that each root conform to the (fixed) polarization.

3.2.1 Isotropic Propagation

The stiffness matrix of fused quartz is

$$\mathbf{c} = \begin{bmatrix} 78.5 & 16.1 & 16.1 & 0 & 0 & 0 \\ 16.1 & 78.5 & 16.1 & 0 & 0 & 0 \\ 16.1 & 16.1 & 78.5 & 0 & 0 & 0 \\ 0 & 0 & 0 & 31.2 & 0 & 0 \\ 0 & 0 & 0 & 0 & 31.2 & 0 \\ 0 & 0 & 0 & 0 & 0 & 31.2 \end{bmatrix} \times 10^9 \text{ N/m}^2 \tag{3.7}$$

and its density is $\rho = 2.2 \times 10^3$ kg/m^3.

Note that in (3.7).

$$c_{12} = c_{11} - 2c_{44}$$

as required by the isotropy of fused quartz. Typical velocity curves are shown in Figure 3.2. Because of the shear degeneracy, there are two curves for any orientation of axes. Because the phase velocity is independent of direction, the curves are circles. (Note that, in all velocity curves, the abscissa and ordinate are labeled with respect to the crystal axis. The phase velocity for a given direction is represented by the magnitude of an imaginary vector from the origin to a point on the curve.)

The fact that there is a shear degeneracy for all directions of propagation has important and interesting consequences. We have shown in

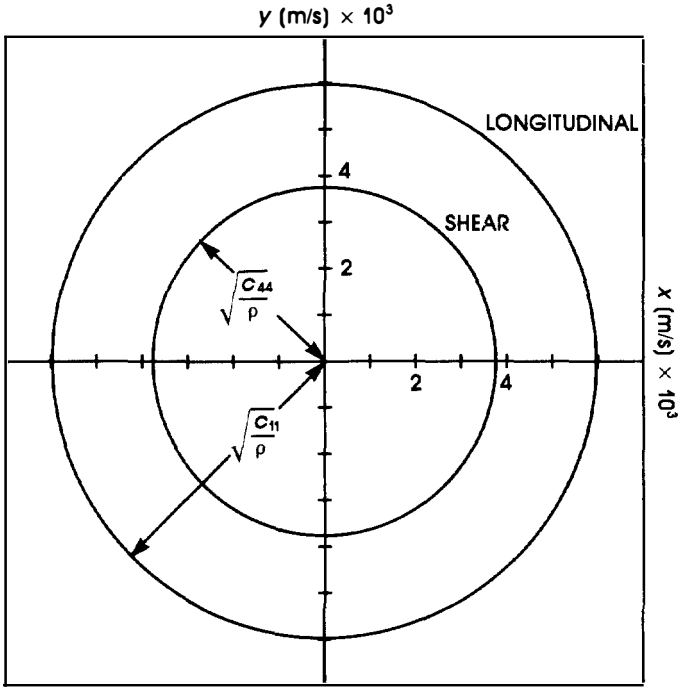

Figure 3.2 Velocity curves of fused quartz in the xy plane. Identical curves are obtained in an arbitrary plane.

Chapter 2 that for each $\hat{\mathbf{l}}$ there are three distinct and mutually perpendicular eigenfunctions or polarizations. These "eigenpolarizations" depend only on the propagation direction for a particular symmetry class. Thus, if a particular eigenpolarization of the crystal is excited (by an external transducer, for example) it will propagate in the medium without changing its orientation. If, however, a polarization is excited that is not an eigenfunction of the crystal, it will decompose into the two "allowed" polarizations and both will propagate. These two modes, which are orthogonally polarized to each other, are the only shear modes that can propagate. If a signal of finite time duration is introduced into the crystal such that it decomposes into two eigenmodes of different phase velocities, both modes may be detected as discrete signals at the other side of the body. Alternatively, if the signal is continuous wave (CW), the polarization of the received signal will generally be rotated with respect to the incident polarization. This is analogous to optic propagation in a glass fiber waveguide in which a complex signal is introduced and propagates as a discrete set of the eigenmodes of the guide. The signal spreads in time, resulting in

signal distortion because the modes generally have different velocities. If, however, both (acoustic) modes have the same velocity, as in the case of a shear degeneracy, they will arrive in phase and will recombine at the output with an identical polarization. Thus, in the case of a shear wave degeneracy, any shear polarization is an eigenpolarization of the crystal. In an isotropic medium, then, all polarizations propagate as eigenfunctions of the body. In other symmetries, degeneracies occur only for certain discrete (usually symmetry) directions.

3.2.2 Cubic Propagation

We first consider gallium arsenide (GaAs):

$$\mathbf{c} = \begin{bmatrix} 119 & 53.8 & 53.8 & 0 & 0 & 0 \\ 53.8 & 119 & 53.8 & 0 & 0 & 0 \\ 53.8 & 53.8 & 119 & 0 & 0 & 0 \\ 0 & 0 & 0 & 59.4 & 0 & 0 \\ 0 & 0 & 0 & 0 & 59.4 & 0 \\ 0 & 0 & 0 & 0 & 0 & 59.4 \end{bmatrix} \times 10^9 \text{ N/m}^2 \qquad (3.8)$$

and $\rho = 5.5 \times 10^3$ kg/m^3. As expected, the stiffness components do not satisfy the isotropic condition. Velocity curves in the *xy* plane are shown in Figure 3.3. Because the major axes are identical, equivalent curves would be obtained in the other principal planes (*xy* and *yz*). We note that only the velocity of the pure shear mode is independent of direction in the *xy* plane. There is a shear mode degeneracy for propagation along the major axes. For all other directions, the velocity of the quasishear mode is less than the pure mode. For this reason, it is sometimes referred to (erroneously) as the slow shear mode, and the pure shear mode is called the fast shear mode.

Consider, however, the case of bismuth germanium oxide (BGO). The relevant stiffness constants are

$$c_{11} = 120 \times 10^9 \text{ N/m}^2, \; c_{12} = 25.5 \times 10^9 \text{ N/m}^2, \; c_{44} = 30.5 \times 10^9 \text{ N/m}^2$$

In this case, the velocity of the pure shear mode is larger than the quasi-mode for all directions except the major axes. Figure 3.4 shows the velocity curves, which include the body diagonal ($\langle 1, 1, 1 \rangle$) for GaAs. This direction exhibits a shear degeneracy and the largest longitudinal velocity (most cubic crystals are stiffest along the body diagonal). The lack of symmetry occurs because the abscissa and the ordinate are not symmetry axes. We also note that there are two more shear degeneracies in this plane. It is

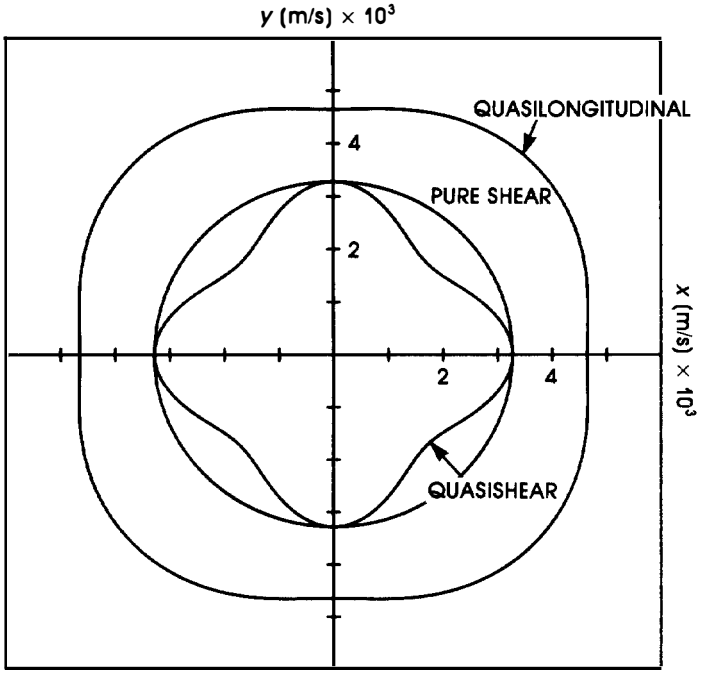

Figure 3.3 Velocity curves of gallium arsenide (cubic) in the *xy* plane (identical curves are obtained in the other principal planes).

not difficult to show that they occur at 70.5° and 125°, and represent the $\langle -1, 1, 1 \rangle$ and $\langle -1, 0, 0 \rangle$ directions.

3.2.3 Tetragonal Propagation

The stiffness matrix for rutile (TiO_2) is

$$\mathbf{c} = \begin{bmatrix} 266 & 173 & 136 & 0 & 0 & 0 \\ 173 & 266 & 136 & 0 & 0 & 0 \\ 136 & 136 & 470 & 0 & 0 & 0 \\ 0 & 0 & 0 & 124 & 0 & 0 \\ 0 & 0 & 0 & 0 & 124 & 0 \\ 0 & 0 & 0 & 0 & 0 & 189 \end{bmatrix} \times 10^9 \text{ N/m}^2 \tag{3.9}$$

and $\rho = 4.3 \times 10^3$ kg/m^3. There are six independent stiffness components. Velocity curves are shown in the *xy* plane in Figure 3.5. Propagation is similar to the cubic case except for the lack of a shear wave degeneracy

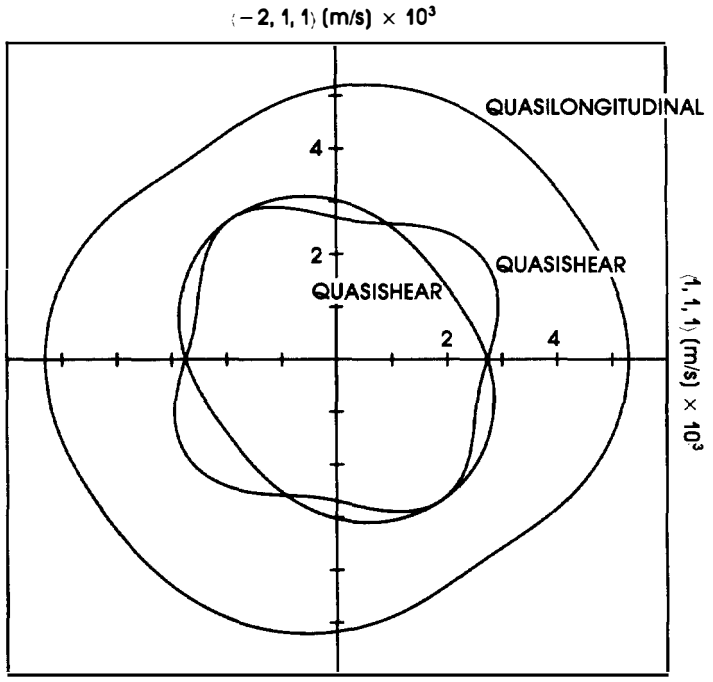

Figure 3.4 Velocity curves of gallium arsenide in the ⟨1, 1, 1⟩-⟨−2, 1, 1⟩ plane. Note the points of shear degeneracy.

along the x- or y-axes. Curves for the xz plane are shown in Figure 3.6. Not shown are the velocity curves in the yz plane, because they are identical to the xz plane curves; the reason for this is that the x- and y-axes have identical stiffness components $c_{13} = c_{23}$. Similar curves for paratellurite (TeO_2) are shown in Figures 3.7 and 3.8. We note that the shape of the curves for similar planes are identical for these two crystals, because the curves are determined entirely by the symmetry of the crystal class.

3.2.4 Paratellurite and Anomalously "Slow" Modes

Paratellurite (TeO_2) is an interesting example of a crystal that does not behave as expected. As a metal oxide with both moderate density ($\rho = 6 \times 10^3$ kg/m^3) and hardness (4 on the mho scale), its acoustic phase velocity should be relatively high. This is correct for propagation along the principal axes. The quasishear mode, however, in the ⟨1, 1, 0⟩ direction, with velocity given by (2.107 is anomalously low due to the proximity of c_{11} and c_{12}. This sharp decrease in phase velocity occurs in some other

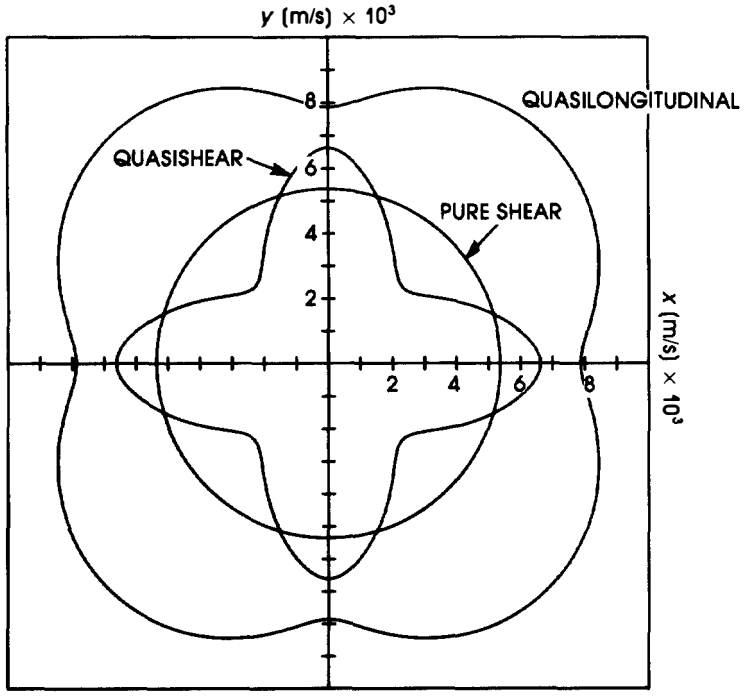

Figure 3.5 Velocity curves of rutile (TiO_2) in the xy plane.

materials, including AgI, Hg_2Cl_2, and InTl. In all these materials, the velocity along the x- and y-axes is not particularly slow, but, for reasons that are not entirely understood, the difference between c_{11} and c_{12} is extremely small. We can envision an extreme situation in which $c_{12} \rightarrow c_{11}$. In this case, the quasishear mode would not propagate at all; we could almost think of the crystal "melting" and transforming itself into a liquid (which does not support shear waves). However, this explanation is not satisfactory because we still have the puzzling problem of the pure shear wave with a velocity that depends on c_{44}. Only in the isotropic approximation does the disappearance of the quasishear mode necessarily require the simultaneous vanishing of the pure shear mode. These anomalously slow waves are extremely important in applications, including long delay lines for storage elements and high resolution acousto-optics, and the understanding and control of this phenomenon is an area of active research.

A second peculiarity of paratellurite is that $c_{66} > c_{11}$. This fact has an interesting consequence for the velocity curves in the xy plane. Because (see (2.101)) the shear and longitudinal velocities along the x- and y-axes depend on c_{66} and c_{11}, respectively, the shear velocity is larger than the

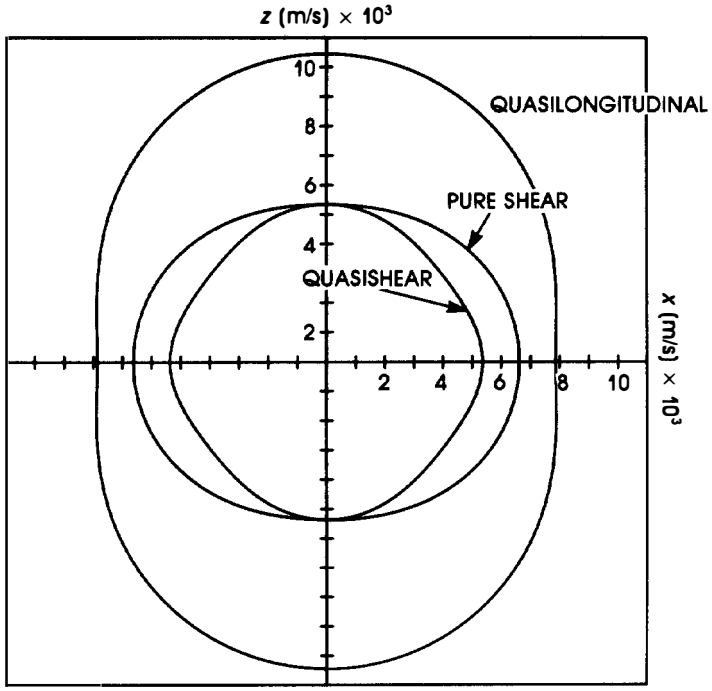

Figure 3.6 Velocity curves of rutile in the *xz* plane. Identical curves are obtained in the *yz* plane.

longitudinal velocity along these axes. This fact, which is not connected to the anomalous behavior along ⟨1, 1, 0⟩, is an exception to the rule that longitudinal velocities are larger than shear velocities. However, following each of the "quasi" curves individually from the ⟨1, 0, 0⟩ to the ⟨1, 1, 0⟩ directions, we find that the longitudinal mode for ⟨1, 0, 0⟩ has become a pure shear mode (the anomalously slow mode) along ⟨1, 1, 0⟩, and the pure shear mode along the *x*-axis has been transformed into a pure longitudinal mode. Indeed, at approximately 8°, both modes deviate from the propagation direction by 45°! Clearly, in this case it is impossible to speak of shear or longitudinal modes at all. However, none of these conclusions contradicts any of our previous discussions. The form of the Christoffel equation guarantees the existence of three *mutually* perpendicular modes; it says nothing about the relation of these modes to the propagation direction, which is determined by the form and values of the stiffness matrix components.

Finally, we investigate the velocity curves of paratellurite in the *xz* plane (which curves are identical to the *yz* curves), as shown in Figure

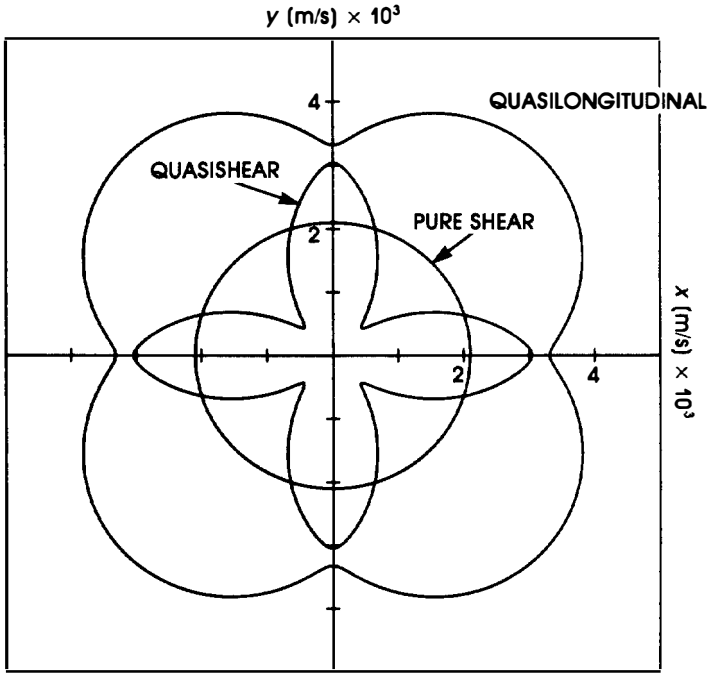

Figure 3.7 Velocity curves of paratellurite (TeO_2) in the xy plane. Note the similarity of their shapes to the curves for rutile.

3.8. Along the x-axis, we recall that the shear mode has a higher velocity than does the longitudinal mode. The longitudinal velocity curve stays longitudinal in this plane, however (although the deviation from the pure mode direction is substantial). Also present are the pure and quasishear modes, but the pure mode is *not* represented by the circular velocity curve as it is in the xy plane. To show this, we consider the Christoffel matrix for tetragonal symmetry in the yz plane. From (2.100), we have

$$\Gamma = \begin{bmatrix} c_{44}l_z^2 + c_{66}l_y^2 & 0 & 0 \\ 0 & c_{11}l_y^2 + c_{44}l_z^2 & (c_{13} + c_{44})l_y l_z \\ 0 & (c_{13} + c_{44})l_y l_z & c_{33}l_z^2 + c_{44}l_y^2 \end{bmatrix} \tag{3.10}$$

The pure shear mode is x-polarized; its stiffness constant is

$$c' = c_{44}l_z^2 + c_{66}l_y^2$$

which clearly depends on the propagation direction varying from c_{66} for y propagation to c_{44} for z propagation. The pure mode has an elliptically shaped velocity curve, and the circular curve in Figure 3.8 (actually, it is not quite a circle) represents the *quasi*shear mode. For tetragonal classes, the pure shear mode has a circular velocity curve only in the xy plane.

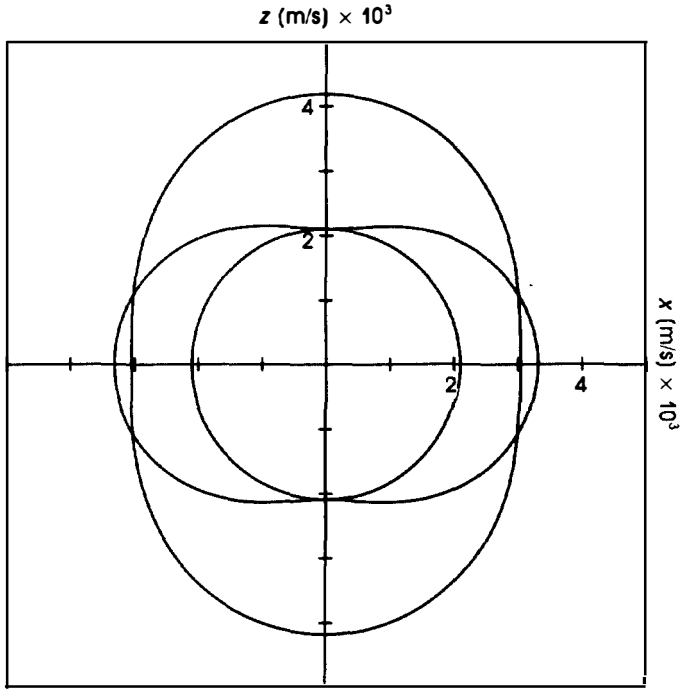

Figure 3.8 Velocity curves for TeO_2 in the xz plane. There is a shear degeneracy not only along z but also at intermediate points.

3.2.5 Orthorhombic Propagation

The stiffness matrix for barium sodium niobate ($Ba_2NaNb_5O_{15}$) is

$$\mathbf{c} = \begin{bmatrix} 239 & 104 & 50 & 0 & 0 & 0 \\ 104 & 247 & 52 & 0 & 0 & 0 \\ 50 & 52 & 135 & 0 & 0 & 0 \\ 0 & 0 & 0 & 65 & 0 & 0 \\ 0 & 0 & 0 & 0 & 66 & 0 \\ 0 & 0 & 0 & 0 & 0 & 76 \end{bmatrix} \times 10^9 \text{ N/m}^2 \tag{3.11}$$

and $\rho = 5.3 \times 10^3$ kg/m^3. Velocity curves for the xy plane are shown in Figure 3.9. In the other principal planes, the curves are quite similar, namely, the shear wave velocity curves are very nearly identical. The "quasishear" degeneracy is due not to the crystal symmetry class but to the particular stiffness component values for which

$$c_{11} - 2c_{44} = 109 \approx 104 = c_{12}$$

Thus, the isotropy condition (2.35) is nearly fulfilled. Likewise, there are no degeneracies along the major axes, but $c_{44} \approx c_{55}$, so there is a near shear degeneracy along the z-axis.

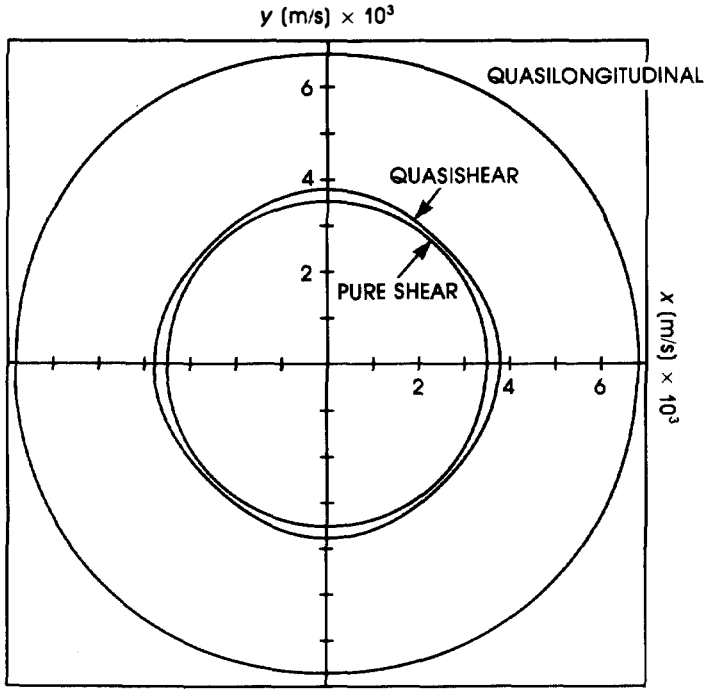

Figure 3.9 Velocity curves of barium sodium niobate in the xy plane. Even though orthorhombic, the curves resemble those of fused quartz because of the relation of the stiffness constants. Of the three curves, only one is pure.

Figures 3.10 and 3.11 show the velocity curves for Rochelle salt in the xy and yz planes. For this crystal, the curves in each principal plane

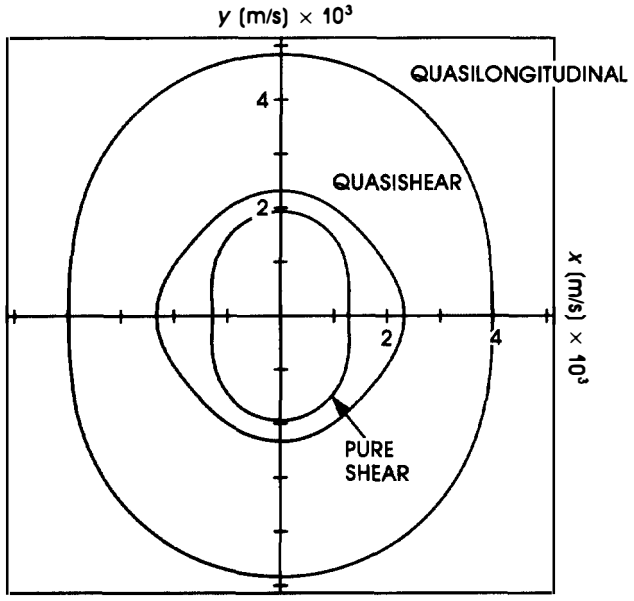

Figure 3.10 Velocity curves of Rochelle salt in the xy plane. The pure mode is represented by the inner curve.

are radically different. The stiffness matrix for this orthorhombic crystal is

$$\mathbf{c} = \begin{bmatrix} 28 & 17.4 & 15 & 0 & 0 & 0 \\ 17.4 & 41.4 & 19.7 & 0 & 0 & 0 \\ 15 & 19.7 & 39.4 & 0 & 0 & 0 \\ 0 & 0 & 0 & 8.7 & 0 & 0 \\ 0 & 0 & 0 & 0 & 2.9 & 0 \\ 0 & 0 & 0 & 0 & 0 & 9.6 \end{bmatrix} \times 10^9 \text{ N/m}^2 \tag{3.12}$$

where $\rho = 1.77 \times 10^3$ kg/m^3. For this crystal, there are no points of shear degeneracy that are obvious from inspection of the stiffness matrix. Thus, curves have dramatically different shapes in the principal planes, and multiple degeneracies appear at intermediate directions rather than along the principal axes. In each plane, however, there is one pure shear mode. Although an inspection of the Christoffel matrix will not clearly tell us which of the two shear velocity curves represents the pure mode in each principal plane, we can easily identify the pure mode curve by finding the velocities along the principal axes.

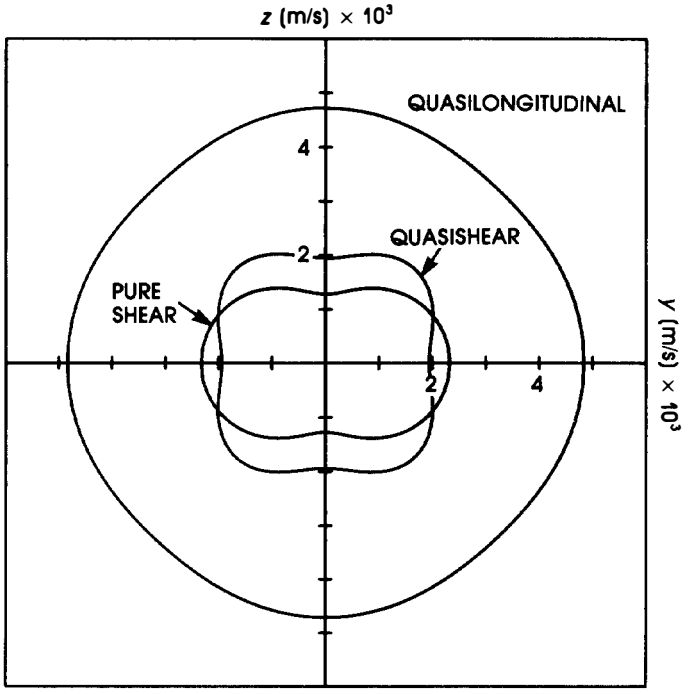

Figure 3.11 Velocity curves of Rochelle salt in the yz plane.

3.3 PROPERTIES OF THE SLOWNESS CURVE

Slowness is a scalar property of an acoustic mode equal to the inverse of the phase velocity of the mode. We can derive a slowness curve from the phase velocity curve by simply inverting the phase velocity for each direction of propagation. To plot the slowness curves using the program CHRISTOFFEL, we form the slowness by inverting the values on lines 4060–4120, and setting the window to fill the screen. Examples of slowness curves for cubic and tetragonal symmetries are shown in Figures 3.12 and 3.13.

Values of slowness range from 10^{-4} s/m (for the longitudinal ⟨1, 1, 1⟩ mode in sapphire) to greater than 3×10^{-3} s/m (for the quasishear ⟨1, 1, 0⟩ mode in Hg_2Cl_2 or InTl).

The utility of the slowness curve comes from the following relations:

$$\delta\hat{\mathbf{k}} \cdot \mathbf{V}_e = 0 \tag{3.13}$$

and

$$\hat{\mathbf{l}} \cdot \mathbf{V}_e = v_a \tag{3.14}$$

where $\mathbf{V}_e$ is a vector describing the velocity of energy propagation (equal to the group velocity). The derivation of (3.13) and (3.14) is given in Born and Wolf [1] and is not repeated here. Equations (3.13) and (3.14) are a property of optic as well as acoustic waves in anisotropic media. In optics, the slowness curve is usually defined as a surface and is called the *wave vector* or, simply, *wave surface*; the effects of the anisotropy are usually quite small when compared with optical inhomogeneities. In acoustics, on the other hand, the effects of inhomogeneities are almost always negligible in high-quality single crystals, and acoustic anisotropy can have extremely important consequences.

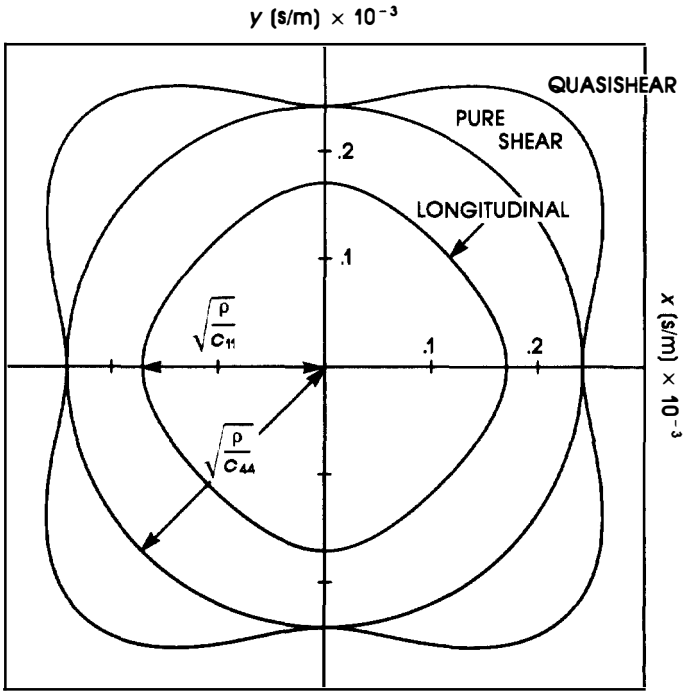

Figure 3.12 Inverse velocity or slowness curves of gallium phosphide in a principal plane. The longitudinal curve is usually the inner curve because it has the highest velocity.

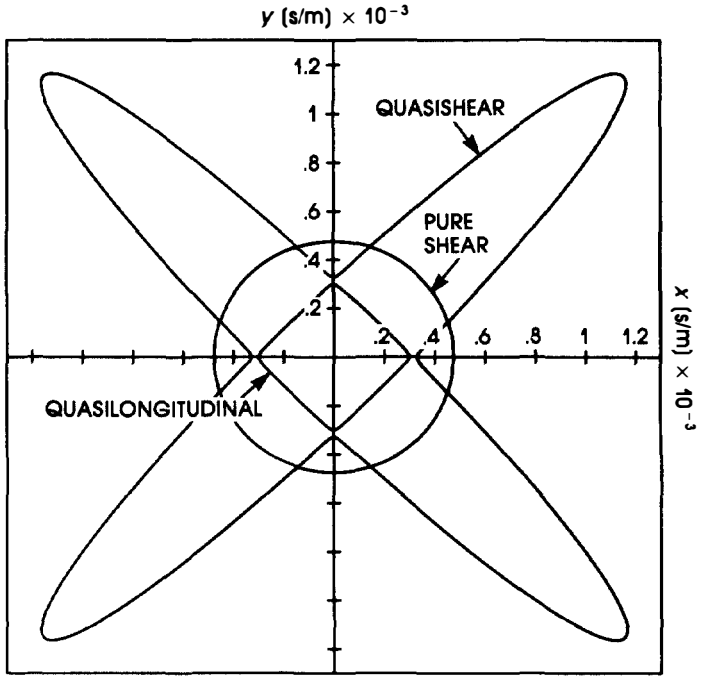

Figure 3.13 Slowness curves of TeO_2 in the xy plane; note the resemblance to the slowness curves of GaP, except that there is no shear degeneracy along x or y. The anomalously slow quasimode has important applications.

3.3.1 Power Flow Angle

Let us examine (3.13) in more detail. Consider a section of an arbitrary slowness curve, as shown in Figure 3.14. The magnitudes of the vectors are (for a given frequency)

$$\left|\frac{\mathbf{k}_1}{\omega}\right| = \frac{1}{v_{a1}} \quad \text{and} \quad \left|\frac{\mathbf{k}_2}{\omega}\right| = \frac{1}{v_{a2}}$$

The direction of the vectors is simply the direction of the normalized propagation vector $\hat{\mathbf{l}}$. In the limit in which $\mathbf{k}_2 \rightarrow \mathbf{k}_1$, the vector $\delta\mathbf{k}/\omega$ becomes *tangent* to the slowness curve; the direction of this tangent vector with respect to the coordinate axes depends on $\hat{\mathbf{l}}$. Equation (3.13) states that

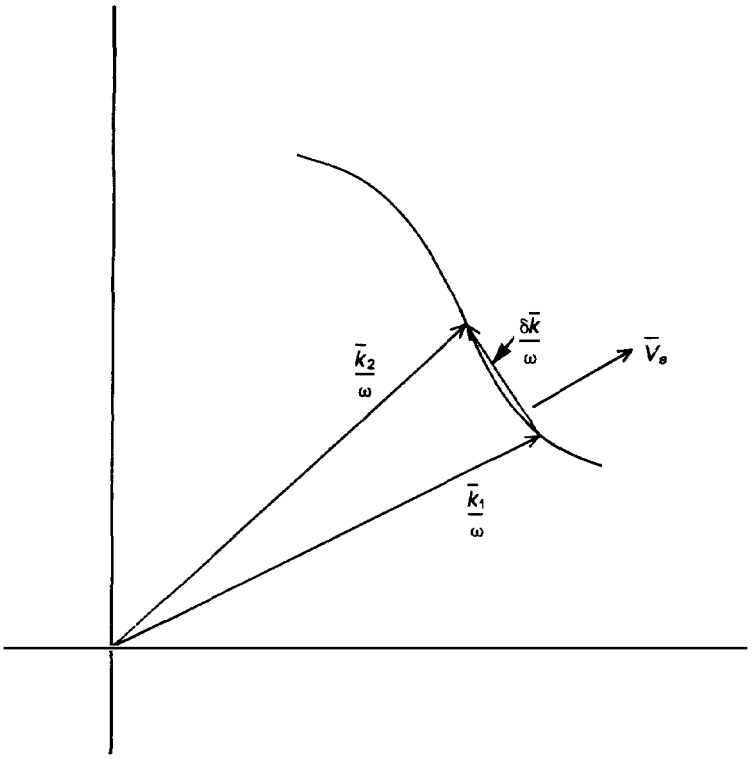

Figure 3.14 Section of slowness curve in the xy plane illustrating the application of (3.13).

the energy velocity is *normal* to the tangent vector at the point of tangency and, thus, normal to the slowness curve (because the scalar product with the tangent vector is zero). Thus, for each point on the slowness curve, the angle between the energy velocity vector and the propagation direction vector depends on the *shape* of the curve. The relation between $\mathbf{V}_e$ and $\hat{\mathbf{l}}$ is given by (3.14):

$$\hat{\mathbf{l}} \cdot \mathbf{V}_e = v_a \quad \text{or} \quad v_a = |\mathbf{V}_e| \cos\phi \tag{3.15}$$

where ϕ is called the *power flow angle*.

For isotropic materials, the slowness curves for all three modes are circles; one quadrant is shown in Figure 3.15. In this case, because the magnitude of v_a is constant for all propagation directions, it is clear that

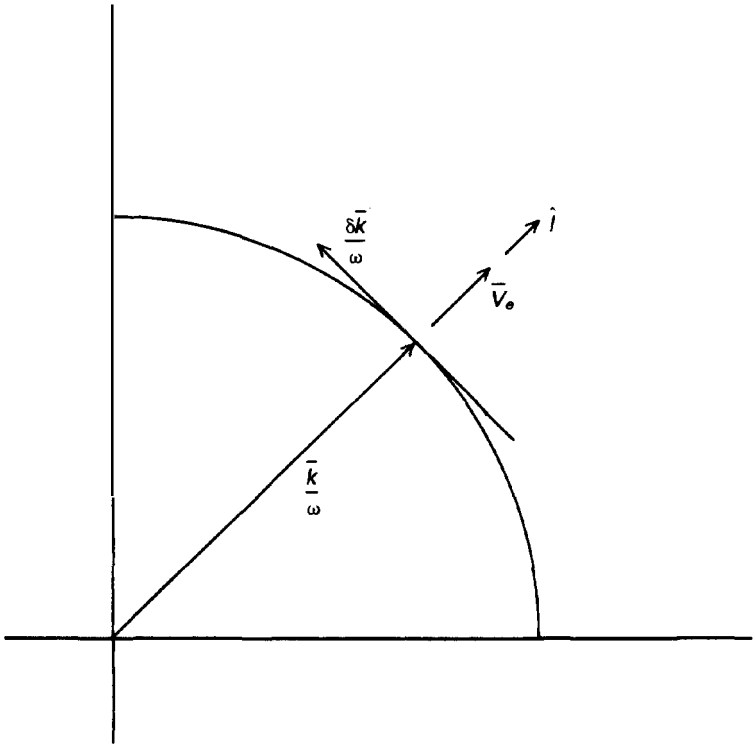

Figure 3.15 Section of slowness curve in which the power flow angle is approximately zero. For this case, $\hat{\mathbf{l}}$ is parallel to $\mathbf{V}_e$.

$\mathbf{V}_e$ is parallel to $\hat{\mathbf{l}}$; the power flow angle is thus zero. Similar conclusions hold for the pure shear modes in all principal planes of cubic symmetry and in the *xy* plane of tetragonal symmetry.

Now consider a section of the slowness curve of the quasi (slow) shear mode of TeO_2 in the *xy* plane (Figure 3.16). In region a, a small change in $\hat{\mathbf{l}}$ causes a large change in the magnitude of the slowness $\mathbf{k}/\omega$. In this region, $\mathbf{V}_e$ is not parallel to $\hat{\mathbf{l}}$, and the power flow angle may be quite large. Instead of propagating along the crystal axis, the energy propagates at a large angle to it, and a transducer placed at the other end of the crystal may not intersect any of the acoustic signal. Obtaining an acousto-optic interaction may also be extremely difficult, because the position of the acoustic beam will be unpredictable. In region b, however, $\hat{\mathbf{l}}$ is parallel to $\mathbf{V}_e$ and $\langle 1, 1, 0 \rangle$ ϕ is zero. Thus, for TeO_2 the energy

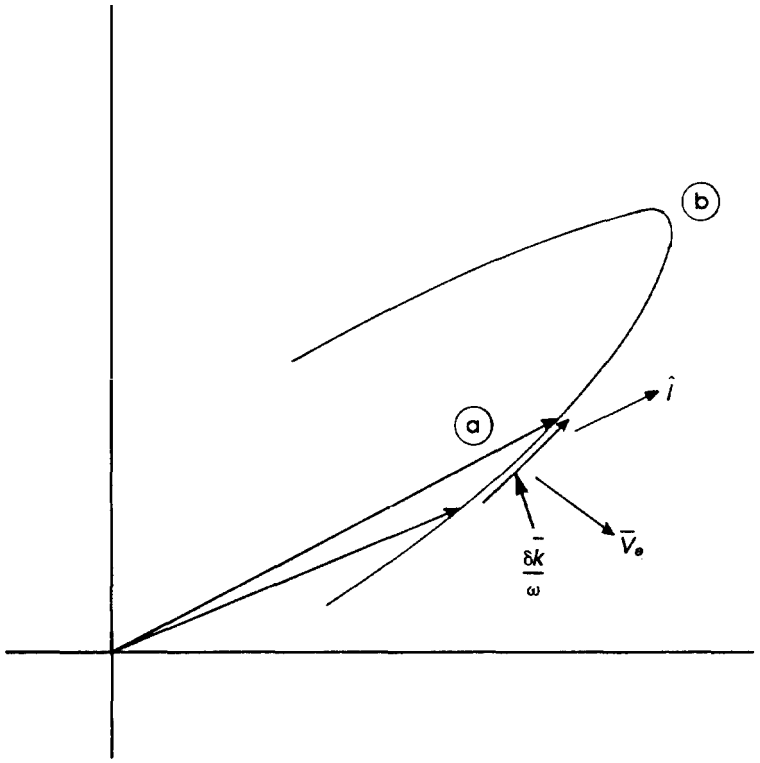

Figure 3.16 Section of slowness curve for which the power flow angle is quite large. Such situations apply to anomalously slow shear mode of paratellurite and cause the energy to walk off the propagation axis.

velocity propagates parallel to the propagation of the phase planes along ⟨1, 1, 0⟩, but if the crystal is miscut, even by a very small angle, the power flow angle can be quite large and cause the acoustic beam to *walk off* from the desired direction (Figure 3.17). The need to cut TeO_2 at precisely 45° greatly increases the cost of this crystal cut.

We can find the power flow angle from the slowness curve by performing the following geometric operations:

1. Form the vector:

$$\frac{\delta \mathbf{k}}{\omega} = \frac{\hat{\mathbf{I}}_2}{V_{a2}} - \frac{\hat{\mathbf{I}}_1}{V_{a1}}$$

2. Normalize the vector.
3. Rotate the vector by 90°.
4. Form the scalar (dot) product with either $\hat{\mathbf{l}}_2$ or $\hat{\mathbf{l}}_1$:

$$\frac{\delta \mathbf{k}}{\omega} \cdot \hat{\mathbf{l}}_2 = \cos\phi$$

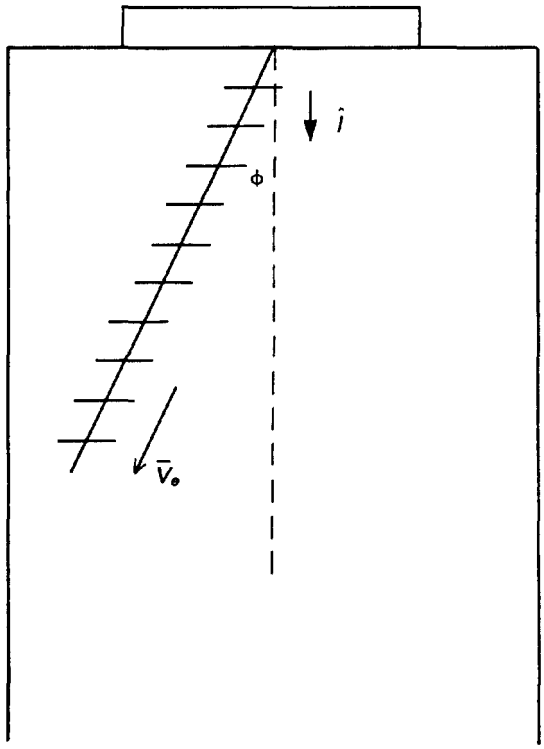

Figure 3.17 Relation of the propagation direction and direction of energy velocity if the power flow angle is not zero.

A program module that calculates the power flow angle is shown in Figure 3.18. The module is placed after line 4120 in the program (in which the three velocities are calculated). The program uses the preceding algorithm and plots the power flow angle as a function of the angle from the (user-defined) abscissa. Because we have chosen a Cartesian plot of ϕ *versus* θ, the window is changed to

Set Window O,PI,O,ϕ_{max}

where ϕ_{max} is the maximum power flow angle. Special care must be exercised in areas of shear degeneracies, because the computer will "jump" from one slowness curve to the other. The problem can be overcome by locating the angles of degeneracy and by directing the program to switch velocities at those points. Figure 3.19 shows the power flow angle of the cubic gallium phosphide. We note that there are only two curves because the pure shear mode has a circular slowness curve, and thus zero ϕ. Identical curves would be obtained in all principal planes. The power flow angle is zero along the symmetry axes and is larger for the quasishear mode than for the quasilongitudinal mode (which is more "circular"). The ⟨1, 1, 0⟩ direction is a symmetry axis for all modes, but inspection of Figure 3.4 shows that the ⟨1, 1, 1⟩ direction is a symmetry axis of the longitudinal mode only, not the shear modes. Figure 3.20 shows the power flow angle curves for rutile in the *xz* plane. Looking at Figure 3.20, we clearly see that all of the curves have finite ϕ. Further, ⟨1, 0, 1⟩ is not a symmetry axis. If the power flow angle of the quasishear mode of TeO_2 is calculated in the *xz* (or *yz*) plane, the maximum value is found to be approximately .5°, which confirms the fact that the slowness curve of this mode is nearly but not perfectly circular.

Now consider the power flow angles of the anomalously slow quasishear modes in the *xy* plane. Slowness curves of three representative crystals are shown in Figure 3.21. Of the three, the slowness curve of silver iodide (AgI) is the "roundest." We would therefore expect that its maximum power flow angle, though large, would be smaller than those of TeO_2 or InTl. Inspecting the power flow curves of AgI and TeO in Figure 3.22 confirms this assertion. A smaller power flow angle eases the tolerances for orienting and cutting the crystal along the ⟨1, 1, 0⟩ direction.

For the ⟨1, 1, 1⟩ direction in cubic crystals, there is a shear degeneracy (as we see from Figure 3.4); both shear modes are pure. Therefore, the longitudinal mode must also be pure because the shear polarization lies in a plane perpendicular to $\hat{\mathbf{l}}$. Green [8] solves this case and writes analytic expressions for the power flow angle. Figure 3.4 shows that ϕ is zero for the longitudinal mode, but finite for the shear modes (thus ⟨1, 1, 1⟩ is not a symmetry direction). Green shows that the energy velocity $\mathbf{V}_e$ generates a conical surface as the polarization is rotated about the axis. This phenomenon is appropriately called *acoustical internal conical refraction*.

In Figures 3.19 and 3.20, we did not distinguish between slowness curves that curved in (usually longitudinal) and those that curve out. Consider the slowness curve of the quasishear mode of a typical cubic crystal (Figure 3.23). In region a, when the wave propagation is along the *y*-axis,

```
4060  LET VEL(1)=(ROOT(1)/DENS)^.5
4090  LET VEL(2)=(ROOT(2)/DENS)^.5
4120  LET VEL(3)=(ROOT(3)/DENS)^.5
4150  IF THETA=0 THEN GOTO 4750
4180  LET A1=(SS(1,1)/VEL(N))-(R4/V(N))
4210  LET B1=(SS(1,2)/VEL(N))-(R5/V(N))
4240  LET NN1=((A1^2)+(B1^2))^.5
4270  LET A1=A1/NN1
4300  LET B1=B1/NN1
4330  LET DT=A1*SS(1,1)+B1*SS(1,2) !DOT PRODUCT
4360  LET PSI=ACOS(DT) !INVERSE COSINE
4390  LET PSI=ABS(PSI)
4420  LET PSI=PSI*180/PI
4450  LET PSI=PSI-90
4480  LET PSI=ABS(PSI)
4510  !PRINT THETA*180/PI,PSI
4540  IF THETA=.5*180/PI THEN GOTO 2230
4570  IF THETA>=PI-.005 THEN
4600  PLOT THETA*180/PI,0
4630  ELSE
4660  PLOT THETA*180/PI,PSI;
4690  END IF
4720  GOTO 4930
4750  PLOT 0,0
4780  LET V(1)=VEL(1)
4810  LET V(2)=VEL(2)
4840  LET V(3)=VEL(3)
4870  LET R4=SS(1,1)
4900  LET R5=SS(1,2)
4930  !CALCULATION IS IN THE X-Y PLANE
4960  NEXT THETA
4990  PLOT 0,0
5020  NEXT N
5050  CLOSE #1
5080  END
```

Figure 3.18 Computer listing for computation of the power flow angle.

the energy velocity is parallel to the propagation direction. If the propagation direction shifts slightly in a direction in the plane, the wave is "pulled" back to the normal (y direction) due to the *curvature* of the slowness curve in this region. In region b, the opposite occurs. The regions should be centered about a symmetry axis so that the focusing (or defocusing) will be symmetric. For cubic or tetragonal classes, we would choose the principal axes and ⟨1, 1, 0⟩, but not ⟨1, 1, 1⟩. Because it is well known that all waves spread due to diffraction and thus change their directions of propagation, it is possible to produce a self-collimating beam if the slowness functions curve inward, as in region a, in just the right degree. This phenomenon is quite similar to electromagnetic propagation in a radially inhomogeneous medium in which the permittivity varies inversely with r^2 (where r is the distance from the axis). In this case, the wave is "pushed" back to the axis by the action of Snell's law, and the medium is said to act as a self-focusing lens; this phenomenon is exploited in the

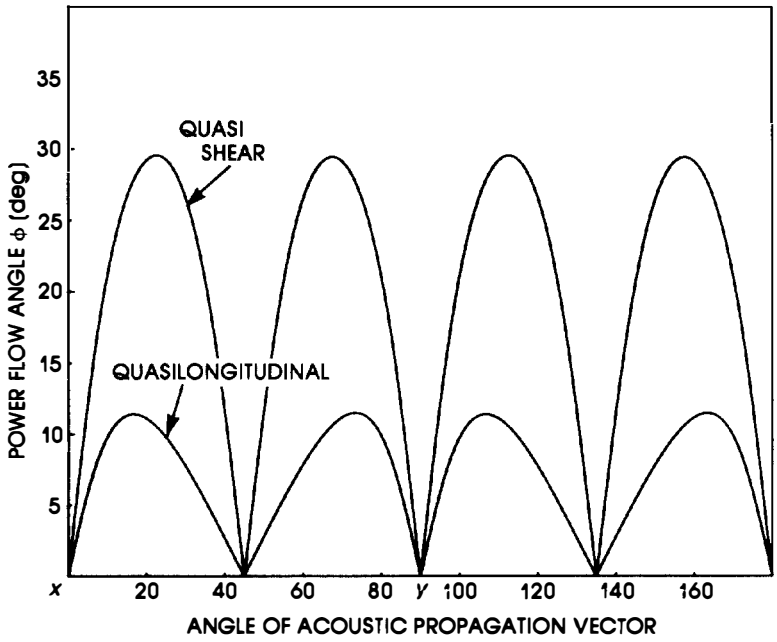

Figure 3.19 Power flow angles of gallium phosphide modes in the xy plane. For the pure shear mode, $\phi = 0$.

design of graded index fiber optics. Here there is no inhomogeneity at all. It is the anisotropy of the crystal and the properties of the slowness curve that act to self-collimate the acoustic energy.

Papadakis and Cohen have examined quantitatively the focusing and defocusing of acoustic waves due to the curvature of the slowness curve [5, 6]. Papadakis has shown that near a symmetry axis the magnitude of the slowness can be written as

$$K^2 = K_0(1 + b\theta^2 + d\theta^4 + \ldots) \tag{3.16}$$

where θ is the angular deviation in radians from the axis usually only the quadratic term is considered. Requiring the curve to be parabolic restricts the maximum value of θ to a few degrees. The condition $b = 0$ represents the isotropic case, in which the slowness curve is circular. An acoustic beam of width H spreads with diffraction angle inversely proportional to

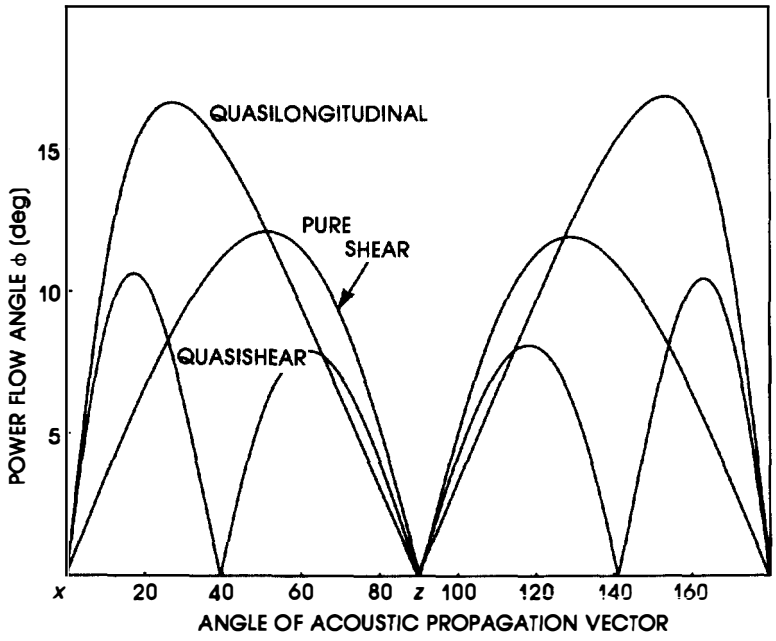

Figure 3.20 Power flow angles of TiO_2 modes in the xz plane.

H. For $b < 0$ (represented by region b in Figure 3.23), the diffraction spread is enhanced by the acoustic anisotropy, whereas for $b > 0$ (region a), diffraction is inhibited. Graphically, the slowness curve for $b < 0$ is more convex, and for $b > 0$ it is more concave, than the circular isotropic curve. Papadakis shows that for $b = 1/2$ the acoustic beam will be self-collimating. For longitudinal modes of cubic symmetry, b is negative over much of the slowness curve in the principal planes, as we can see from Figure 3.12 for gallium arsenide. An exception is the important ⟨1, 1, 0⟩ direction for which $b \approx +.2$, so some collimation results. Cohen points out that b seems to be restricted to values less than 1/2 for longitudinal modes, so it is not possible to find a self-collimating direction. In Chapter 4, we give an exception to this rule. For shear modes, b varies over a much greater range than it does for longitudinal modes. For the pure shear mode (in the principal planes), $b \equiv 0$. For the quasishear mode, b varies from a large negative value (along ⟨1, 1, 0⟩) to a positive value of approximately

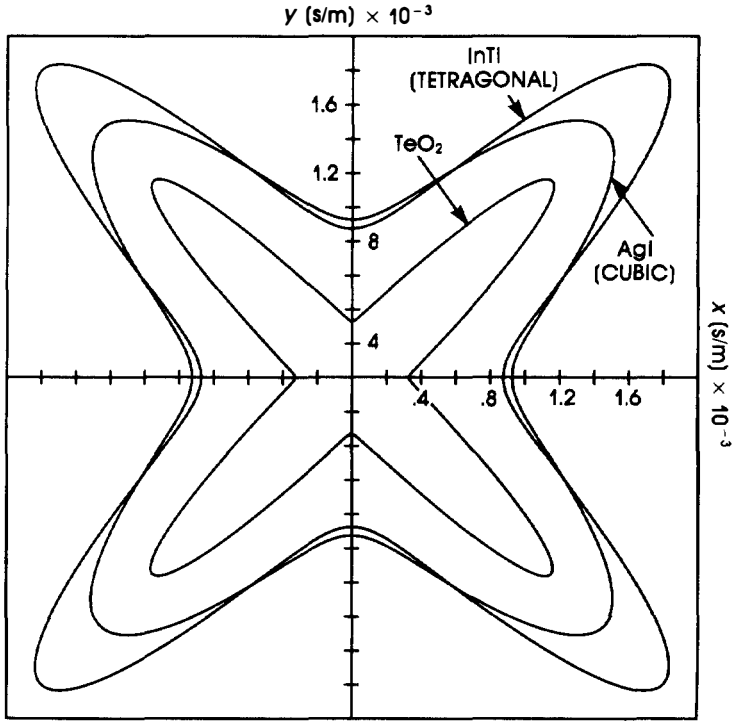

Figure 3.21 Anomalously slow (quasi) shear mode of three representative crystals in the xy plane.

1.2 along the principal axes. For these directions, focusing of the beam occurs.

Hecht and Petrie [7] have considered the problem of finding symmetry directions for which $b \approx 1/2$. They analyzed the slowness curves for the fast shear mode in the $\langle 1, 1, -2\rangle$ - $\langle 1, -1, 0\rangle$ plane of gallium phosphide and found that, around the $\langle 1, -1, 0\rangle$ axis, $b \approx .487$. Experiments confirmed that along this axis the acoustic beam is indeed self-collimating. Unfortunately, it is much easier to analyze the curvature of the slowness curves than to find a particular curvature; this procedure must be done by trial and error because the curvature depends not only on the symmetry class but also on the components of the stiffness matrix. We will return to this configuration in Chapter 8, where we examine the performance advantages of using a self-collimating beam as an acousto-optic device.

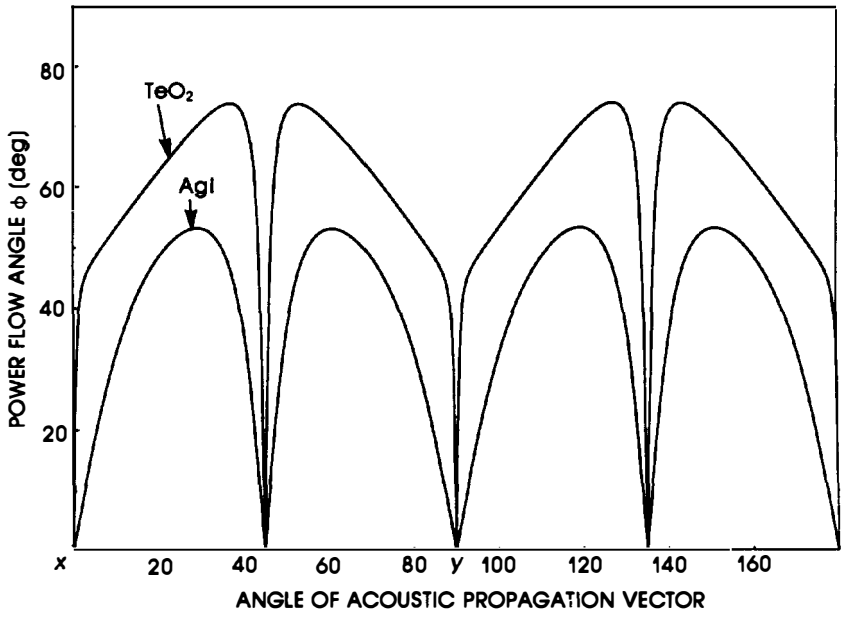

Figure 3.22 Power flow angles for TeO_2 and AgI in the xy plane. The steepness of the slowness peak in TeO_2 results in larger ϕ.

3.3.2 Ray Velocity Curves

We have seen that the energy or ray velocity is found from (3.13) and (3.14). Clearly, if $\phi = 0$ ($\mathbf{l}$ is parallel to $\mathbf{V}_e$), then $|\mathbf{V}_e| = v_a$; this is true if the slowness curves are circles (isotropic crystals and the pure shear mode in cubics). For general symmetries, there are usually points for which the power flow angle ϕ is zero. Consider, for example, the quasishear mode in cubic symmetry in the xy plane (Figure 3.24). At points a and b, $\phi = 0$; likewise at points a and c, the ray velocity has only an x component. It is also clear that $|\mathbf{V}_{e_3}| < |\mathbf{V}_{e_1}|$.

We can use these facts to construct geometrically the ray surface curves. These curves are plots of the energy velocity as a function of propagation direction. A computer module that calculates the components of the ray velocity (recall that the ray velocity is a vector) is easily determined from the power flow calculation. The magnitude of $\mathbf{V}_e$ is given by

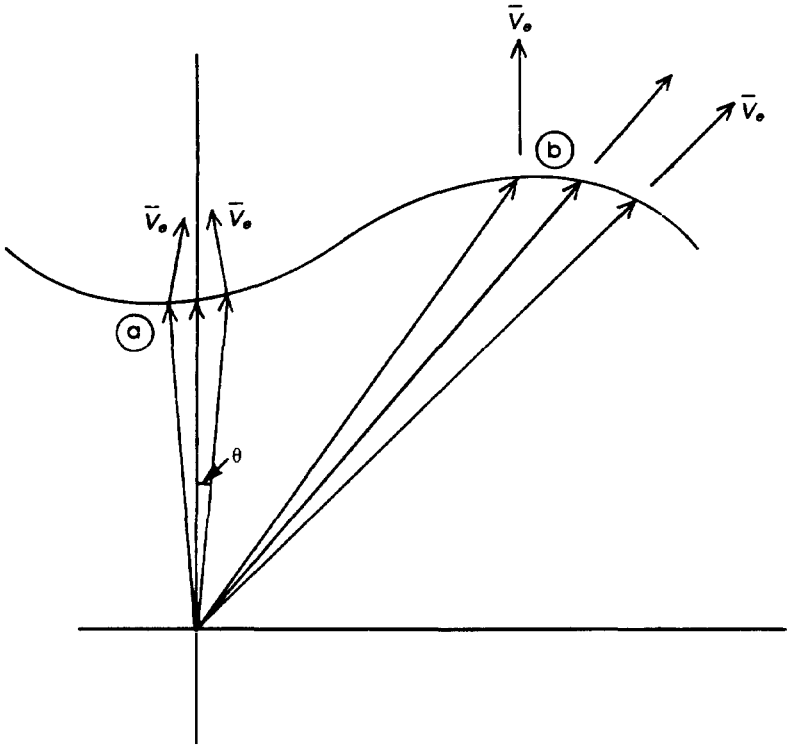

Figure 3.23 The shape of the slowness curves causes acoustic energy to spread (region b) or to focus (region a). It is possible to find points such that the beam is perfectly collimated in certain crystals.

(3.14). Thus, we first calculate the power flow angle as in Figure 3.18, and then we determine the components along the abscissa and the ordinate. Typical ray surface curves are shown in Figure 3.25 for cubic gallium arsenide in the *xy* plane. Note that for the pure shear mode, the ray surface and phase velocity curves are identical because the power flow angle is everywhere zero. Figures 3.26 and 3.27 show the ray surface and phase velocity curves for the quasishear modes of TiO_2 and TeO_2 in the *xy* plane. We note that along the symmetry axes (i.e., the principal axes and ⟨1, 1, 0⟩, where $\phi = 0$) the two velocities have equal magnitudes.

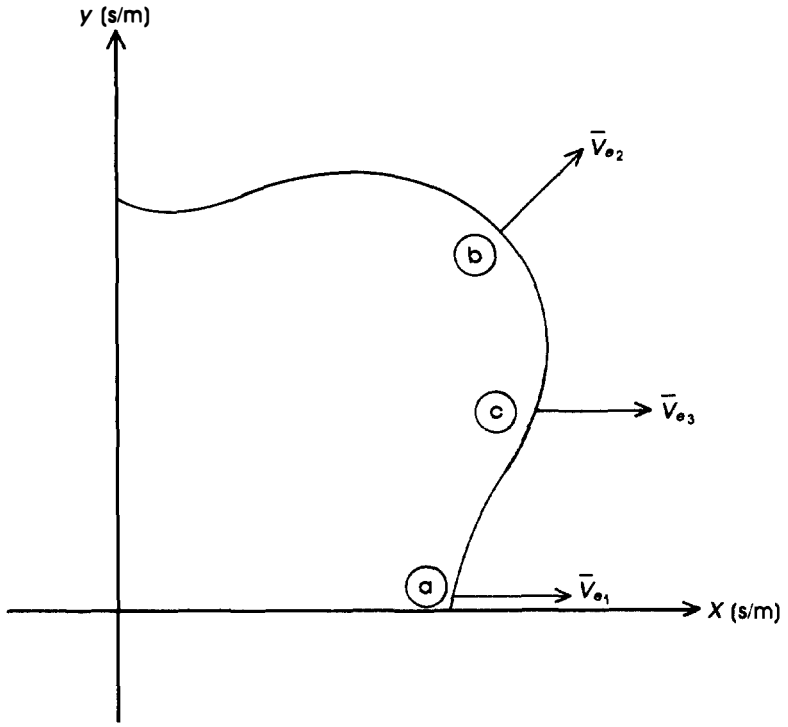

Figure 3.24 The shape of the slowness curves causes the energy velocity to propagate in the x direction at points a and c. This behavior results in a ray surface with sharp lobes.

3.4 DEVIATION ANGLE FROM PURE MODE

Thus far, we have not commented on the relation between $\hat{\mathbf{l}}$ and the polarizations (the eigenvectors), other than to calculate explicitly some special cases in which $\mathbf{l}$ is either parallel (longitudinal mode) or perpendicular (shear mode) to the polarizations. The Christoffel matrix is symmetric, so the eigenvalues are real and the three eigenvectors are mutually perpendicular. As we have previously commented, however, $\hat{\mathbf{l}}$ is *not* required to be parallel or perpendicular to the polarizations, and in general

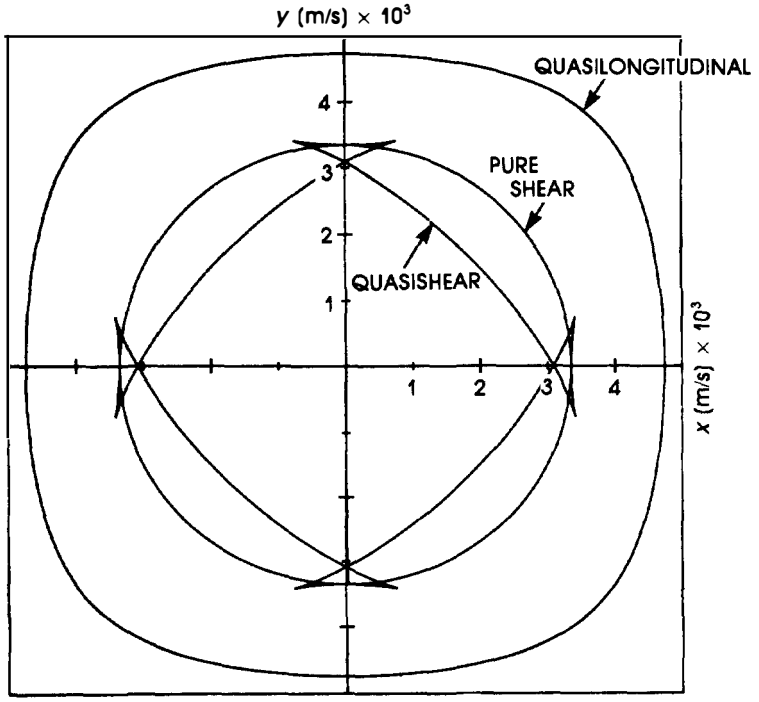

Figure 3.25 Ray surface curves for gallium arsenide in the xy plane. The pure shear mode is circular, but the quasishear mode has lobes characteristic of a slowness curve that bow in.

it is not. In all the cases considered in this chapter, for example, propagation along the principal axes has yielded pure modes. This is not the case for all symmetry systems, and, as we shall see in Chapter 4, for the trigonal classes the deviation angles can be quite large for propagation along the y-axis. In general, acoustic modes are "quasi" modes. The deviation between the "pure" (parallel or perpendicular) and the true directions is quite important, although it is generally quite difficult to solve in closed form.

A computer program to calculate the deviation angle in the xy plane is shown in Figure 3.28. To find the angle of deviation, we must know not only the propagation direction (which is calculated in line 2620 of Figure 3.1) but also the (normalized) polarization. The latter calculation is not

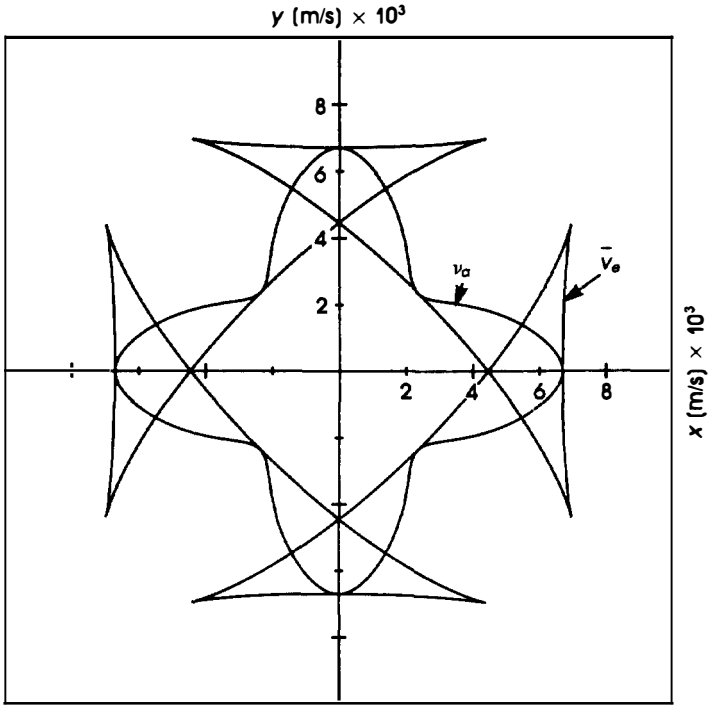

Figure 3.26 Ray surface and phase velocity curves of TiO_2 in the *xy* plane. The curves are degenerate along the principal axes and at ⟨1, 1, 0⟩, where $\phi = 0$.

required in constructing the velocity, slowness, or power flow curves, and is generally quite cumbersome to perform in closed form. As shown in Chapter 2, to find the eigen*functions*, we substitute each *eigenvalue* λ into the characteristic equation in turn. Each substitution results in a set of three equations, of which only two are independent. In all of the classes we have studied, one of the shear modes has been a pure mode in the principal planes. This fact dramatically simplifies the calculation by reducing the order of the characteristic equation from 3 to 2 and allowing the components of the polarization to be written in a simple closed form (lines 4210–4570).

A plot of the deviation for cubic crystals is shown in Figure 3.29. We note that only one curve is shown, because the deviation angle for the

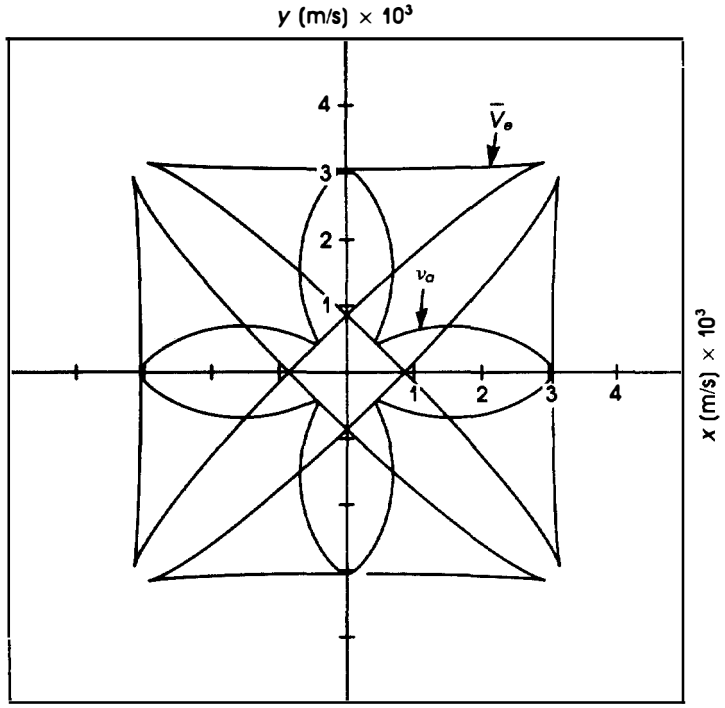

Figure 3.27 Ray surface and phase velocity curves of TeO_2 in the xy plane. Note the similarity in their shapes to those of TiO_2.

pure mode is, by definition, zero, and the three modes are mutually perpendicular. Further, the two polarizations of the quasimodes lie in the xy plane because the pure mode is polarized along z (a similar situation occurs for optic modes, of which there are only two). The form of the deviation curves is quite similar to that of the power flow angle. The two phenomena are not necessarily linked, however. See Figure 3.30, which shows the deviation angle for paratellurite in the yz plane. In this case, even though the velocity curve is nearly a circle, the deviation angle is quite large.

```
4060  LET VEL(1)=(ROOT(1)/DENS)^.5
4090  LET VEL(2)=(ROOT(2)/DENS)^.5
4120  LET VEL(3)=(ROOT(3)/DENS)^.5
4150  !THIS ROUTINE FINDS THE EIGENVECTORS IN THE X-Y PLANE
4180  LET T33(2,2)=T33(2,2)-ROOT(1)
4210  LET VV(1,1)=1
4240  LET VV(2,1)= -T33(2,1)/T33(2,2)
4270  LET VN=(1+VV(2,1)*VV(2,1))^.5
4300  LET VV(1,1)=1/VN
4330  LET VV(2,1)=VV(2,1)/VN
4360  LET VV(3,1)=0
4390  !THE PURE SHEAR MODE, VV(I,2), IS Z POLARIZED IN THE X-Y PLANE
4420  LET VV(1,2)=0
4450  LET VV(2,2)=0
4480  LET VV(3,2)=1
4510  LET VV(1,3)=VV(2,1)
4540  LET VV(2,3)=-VV(1,1)
4570  LET VV(3,3)=0
4600  !PRINT VV(1,3),VV(2,3),VV(3,3)
4630  LET DOT=COS(THETA)*VV(1,1)+SIN(THETA)*VV(2,1)
4660  LET DOT = ABS(DOT)
4690  LET ALPHA=ACOS(DOT)
4720  !PRINT ALPHA*180/PI,THETA*180/PI
4750  PLOT THETA*180/PI,ALPHA*180/PI;
4780  NEXT THETA
4810  CLOSE #1
4840  END
```

Figure 3.28 Program listing for computation of the deviation angle from pure mode directions in the *xy* plane when one mode is pure.

PROBLEMS

3.1 In Figure 3.4, there are two shear degeneracies in the ⟨1, 1, 1⟩-⟨−2, 1, 1⟩ plane. They occur for the directions ⟨−1, 1, 1⟩ and ⟨−1, 0, 0⟩. Show that these directions are in the plane. Show that these directions make angles of 70.5° and 125°, respectively, with the ⟨1, 1, 1⟩ axis.

3.2 Confirm that the value of b is approximately .48 along ⟨1, −1, 0⟩ for gallium phosphide in the ⟨1, 1, 2⟩-⟨1, −1, 0⟩ plane.

3.3 Find the value of b for propagation along the x-axis for the quasishear mode in TeO_2.

3.4 Plot the velocity curves for barium sodium niobate in the xz and yz planes.

3.5 Plot the velocity curves for Rochelle salt in the xz plane.

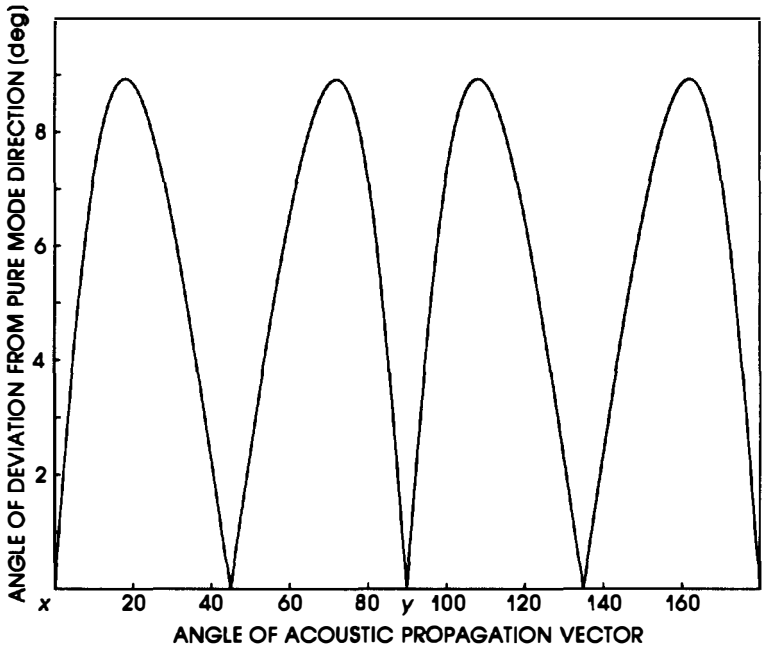

Figure 3.29 Deviation angles for the quasimodes in gallium phosphide. Only one curve is shown because the deviation angles of both quasimodes are equal.

REFERENCES

1. M. Born and E. Wolf, *Principles of Optics,* Pergamon, London, 1975.
2. C. Jen, G. Farnell, E. Adler, and J. Slaboszewicz, "Interactive Computer-Aided Analysis of Bulk Acoustic Waves Using a Personal Computer," *Proc. IEEE Ultrasonics Symp.,* 430 (1984).
3. C. Jen, G. Farnell, E. Adler, and J. Oliveira, "Interactive Computer-Aided Analysis for Bulk Acoustic Waves in Materials of Arbitrary Anisotropy and Piezoelectricity," *IEEE Trans. Sonics and Ultrasonics* **SU-32,** 56, (1985).
4. D. Chung, D. Gunton, and G. Saunders, "Ultrasonic Study of Phonon Mode Softening and Melting in Indium-Thallium Alloys," *Phys. Rev. B***13** (6), 3239 (1976).

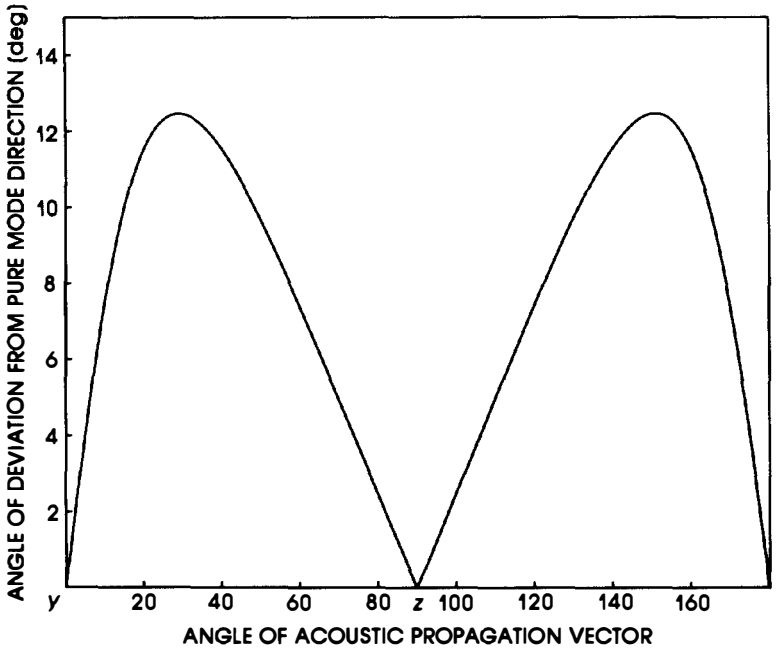

Figure 3.30 Deviation angle for quasimode TeO_2 in the *yz* plane. The quasishear mode is not pure even though the power flow angle is nearly zero.

5. G. Papadakis, "Ultrasonic Diffraction Loss and Phase Change in Anisotropic Materials," *J. Acoustic Society of America* **10,** 863 (1966).
6. M. Cohen, "Optical Study of Ultrasonic Diffraction in Anisotropic Media," *J. Applied Physics* **38** (10), 3821 (1967).
7. D. Hecht and G. Petri, "Acousto-Optic Diffraction from Acoustic Anisotropic Shear Modes in Gallium Phosphide," *Proc. IEEE Ultrasonics Symp.,* 474 (1980).
8. R. Green, *Ultrasonic Investigation of Mechanical Properties,* Academic Press, New York, 1973.
9. J. Murphy and M. Gad, "A Versatile Program for Computing and Displaying Bulk Acoustic Wave Properties of Anisotropic Crystals," *Proc. IEEE Ultrasonics Symp.,* 172 (1978).